Hsu et al. Nanoscale Research Letters (2015) 10:50
DOI 10.1186/s11671-015-0776-8

Nanoscale Research Letters
a SpringerOpen Journal

NANO EXPRESS Open Access

Single-crystalline chromium silicide nanowires and their physical properties

Han-Fu Hsu[1], Ping-Chen Tsai[1] and Kuo-Chang Lu[1,2*]

Abstract

In this work, chromium disilicide nanowires were synthesized by chemical vapor deposition (CVD) processes on Si (100) substrates with hydrous chromium chloride ($CrCl_3 \cdot 6H_2O$) as precursors. Processing parameters, including the temperature of Si (100) substrates and precursors, the gas flow rate, the heating time, and the different flow gas of reactions were varied and studied; additionally, the physical properties of the chromium disilicide nanowires were measured. It was found that single-crystal $CrSi_2$ nanowires with a unique morphology were grown at 700°C, while single-crystal Cr_5Si_3 nanowires were grown at 750°C in reducing gas atmosphere. The crystal structure and growth direction were identified, and the growth mechanism was proposed as well. This study with magnetism, photoluminescence, and field emission measurements demonstrates that $CrSi_2$ nanowires are attractive choices for future applications in magnetic storage, photovoltaic, and field emitters.

Keywords: CVD; Chromium silicide nanowires; Field emission; Ferromagnetic property

Background

Recently, transition metal silicide nanowires have been widely studied [1-9] for their utilization in semiconductor device technologies. Low-resistivity silicides, such as $TiSi_2$, $CoSi_2$, and NiSi, have been applied for interconnection in CMOS devices [10]. The group of refractory semiconducting silicides, composed of silicon and metals, have different physical properties that are useful and importantly meaningful. Among them, semiconducting silicides, such as $CrSi_2$ and ß-$FeSi_2$, with a narrow energy gap (0.1 to 0.9 eV) have been extensively investigated for their potential use in silicon-integrated optoelectronic devices [11] such as LEDs [12,13] and IR detectors [14]. In particular, $CrSi_2$ is a narrow bandgap (0.35 eV) semiconductor [15-17], offering applications in the Schottky barrier solar cell technology [18]. Hexagonal $CrSi_2$ with a C40-type structure has a high melting point and excellent resistance to oxidation, deformation, and stretching, being considered to be a potential structural material for aerospace and energy generation industries [19]. Additionally, it is a thermoelectric conversion component that could be applied to generate electric power at high temperatures [20]; the figure of merit (ZT) of $CrSi_2$ has been measured to be 0.25 at 900 K [21]. $CrSi_2$ also has good field emission with relatively low work function (3.9 eV) [22] as compared with generally studied field emission materials such as CNTs (5 eV) [23] and ZnO (5.3 eV) [24]. With excellent intrinsic properties of $CrSi_2$, one-dimensional $CrSi_2$ nanowires are expected to improve field emission performances by bulk and thin film $CrSi_2$. Though there have been some previous studies on $CrSi_2$ nanowires [25-28], two special aspects can be found in this research. Firstly, we conducted a more systematic study on the influences of each processing parameter on growth. Secondly, we provided a low-cost and simple method to synthesize high-quality $CrSi_2$ nanowires with very good physical properties.

Methods

In our experiments, we synthesized chromium disilicide nanowires with chemical vapor deposition (CVD) processes. Single-crystal Si (001) wafers, the native oxide of which was etched by BOE solution, were substrates. The metal source was from hydrous chromium chloride ($CrCl_3 \cdot 6H_2O$) powders, and the flow gas is Ar gas

* Correspondence: gkclu@mail.ncku.edu.tw
[1]Department of Materials Science and Engineering, National Cheng Kung University, No.1, University Rd, Tainan 701, Taiwan
[2]Center for Micro/Nano Science and Technology, National Cheng Kung University, No.1, University Rd, Tainan 701, Taiwan

(99.99%). The $CrCl_3 \cdot 6H_2O$ powders were put in the upstream zone of the furnace, where the temperature ranged from 700°C to 800°C, while the silicon (001) substrates were put in the downstream zone with the same temperature range. During the growth process, with oxygen environment, $CrSi_2$ nanowires may transform to be $CrSi_2$(core)/SiO_2(shell) nanowires due to oxidation. To understand what factors influence the growth of chromium disilicide nanowires, we varied reaction time and temperatures of substrates and the metal source. Scanning electron microscopy (SEM), X-ray diffraction (XRD), and transmission electron microscopy (TEM) studies were conducted for morphology observation and structure identification of the nanowires. Additionally, physical properties, including magnetism (SQUID), photoluminescence (PL), and field emission (Keithley-237), were measured.

Results and discussion

In this work, we controlled different parameters to realize how they influence the nanowires' growth, morphology, and physical properties. With source and substrate at 700°C and the flow gas of 120 sccm, we obtained dense $CrSi_2$ nanowires with a length of approximately 20 μm as shown in Figure 1a by chemical vapor deposition. Interestingly, in Figure 1b, the nanowires grew from the particle with almost coherent growth direction and the morphology was rare. XRD analysis in Figure 1c shows (111), (003), and (112) major plane peaks, indicating that the nanowires have a C40 hexagonal structure. The TEM image of Figure 2a shows that the nanowires are 10 to 50 nm in diameter. In Figure 2b, the high-resolution transmission electron microscopy (HRTEM) image and the corresponding fast Fourier transform (FFT) pattern in the inset identifies the materials to be single-crystal $CrSi_2$ nanowires of a hexagonal structure with lattice constants, $a = 0.4428$ nm and $c = 0.6369$ nm (JCPDS card no. 35–0781); the growth direction is [001], and the interplanar spacing of plane (003) is 0.2098 nm. Additionally, we tried 750°C with hydrogen as reducing atmosphere and obtained Cr_5Si_3 nanowires of approximately 10 μm in length and of a different morphology as shown in Figure 1d. In Figure 1e, we found that the nanowires grew from nanoparticles again. XRD analysis in Figure 1f shows two phases, $CrSi_2$ and Cr_5Si_3; for further investigation on the atomic structures of the nanowires, we conducted TEM analysis as shown in Figure 2. From the TEM image of Figure 2c, the nanowire was of approximately 80 nm in diameter. The HRTEM image and the corresponding FFT pattern in the inset of Figure 2d confirm that the single-crystal Cr_5Si_3 nanowire has a BCT D8m structure with lattice constants, $a = 0.9165$ nm and $c = 0.4638$ nm (JCPDS card no. 51–1357); also, the nanowire is with

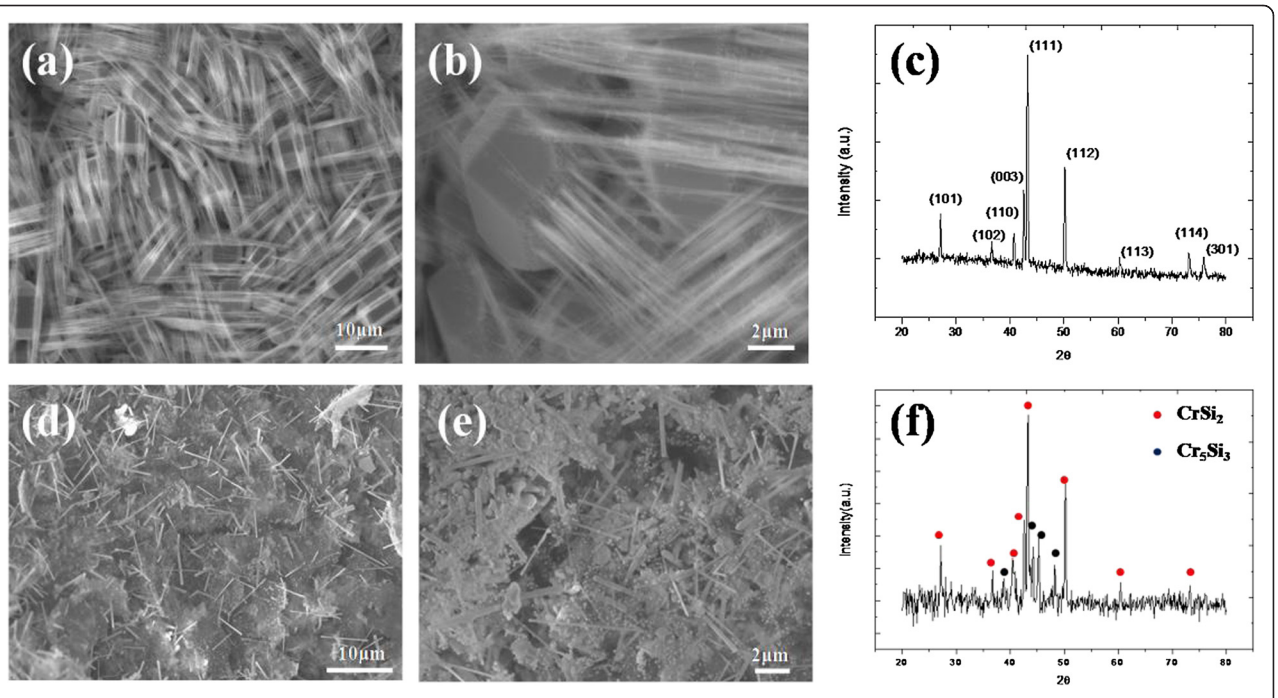

Figure 1 SEM images and XRD analysis of chromium silicide nanowires. (a) Low magnification, **(b)** high-resolution SEM images, and **(c)** XRD analysis of $CrSi_2$ nanowires grown at 700°C. **(d)** Low magnification, **(e)** high-resolution SEM images and **(f)** XRD analysis of Cr_5Si_3 nanowires grown at 750°C with H_2 atmosphere.

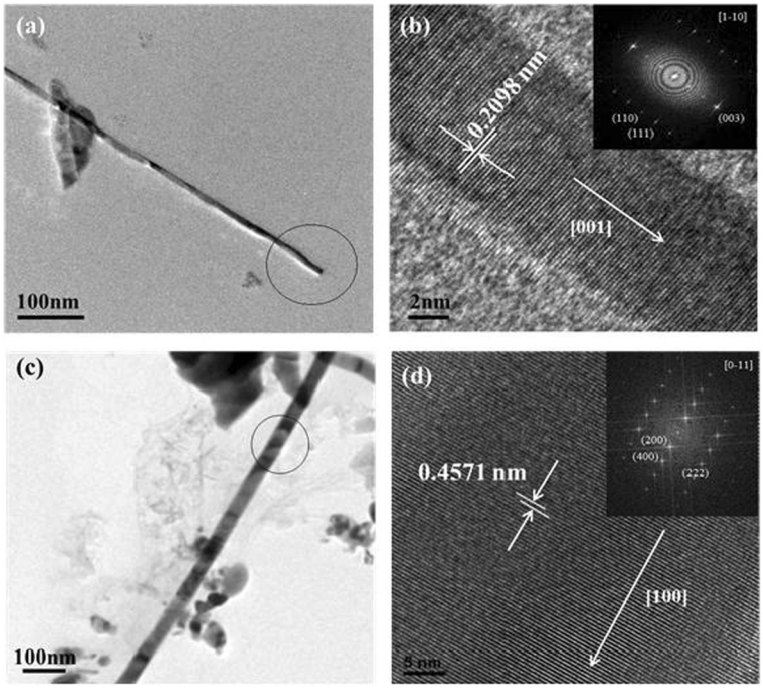

Figure 2 TEM analysis of chromium silicide nanowires. (a) Low magnification, **(b)** high-resolution TEM images of $CrSi_2$ nanowires grown at 700°C. The inset in **(b)** shows the corresponding fast Fourier transform (FFT) pattern with a zone axis of [1–10]. **(c)** Low magnification, **(d)** high-resolution TEM images of Cr_5Si_3 nanowires grown at 750°C. The inset in **(d)** shows the corresponding FFT pattern with a zone axis of [0–11].

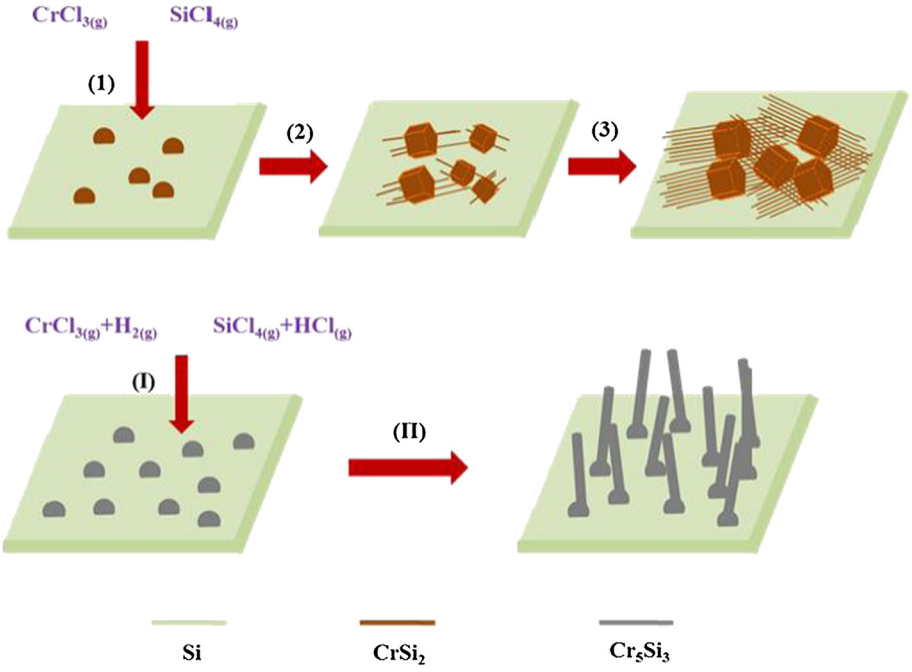

Figure 3 Schematic illustration of the growth mechanism. (1) $4CrCl_{3(g)} + 11Si_{(s)} \rightarrow 4CrSi_{2(s)} + 3SiCl_{4(g)}$; $4SiCl_{4(g)} + 2CrCl_{3(g)} \rightarrow 2CrSi_{2(l)} + 11Cl_{2(g)}$. (2) Growth of $CrSi_2$ particles and nanowires. (3) High-density $CrSi_2$ nanowires. (I) $10CrCl_{3(g)} + 12Si_{(s)} + 3H_{2(g)} \rightarrow 2Cr_5Si_{3(s)} + 6SiCl_{4(g)} + 6HCl_{(g)}$. (II) Growth of Cr_5Si_3 nanowires.

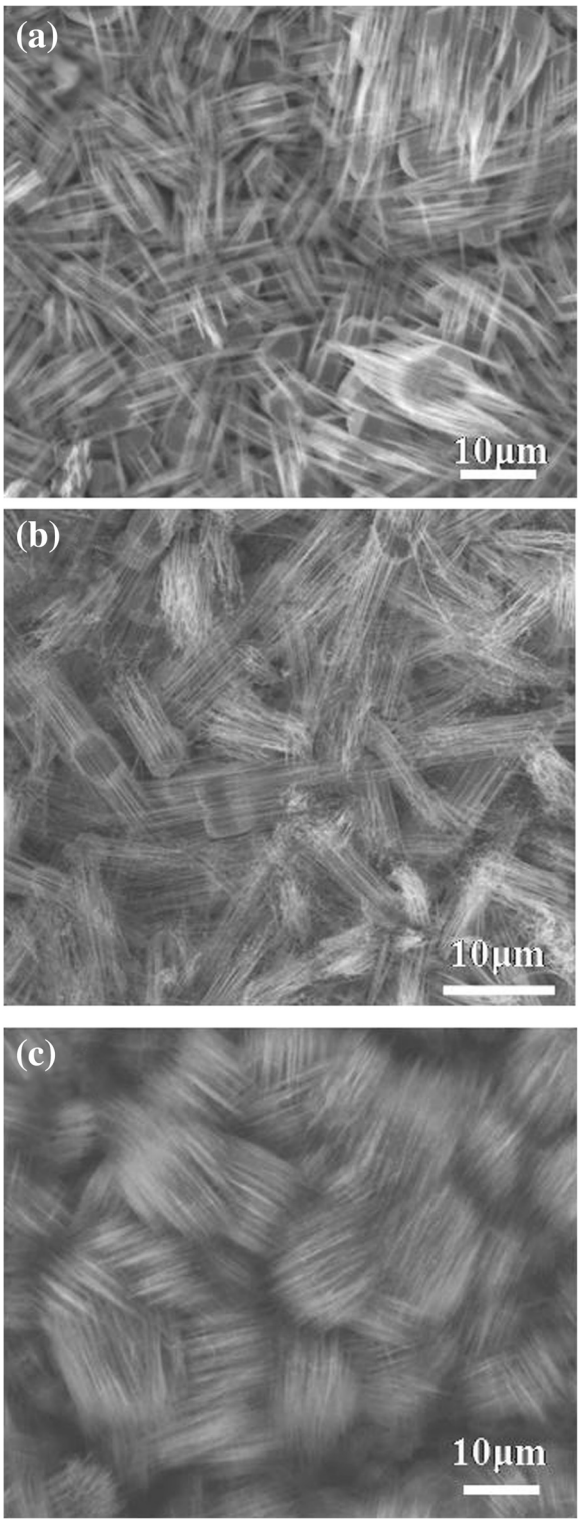

Figure 4 SEM images of $CrSi_2$ nanowires at different heating times of (a) 1.5, (b) 4, and (c) 12 h, respectively.

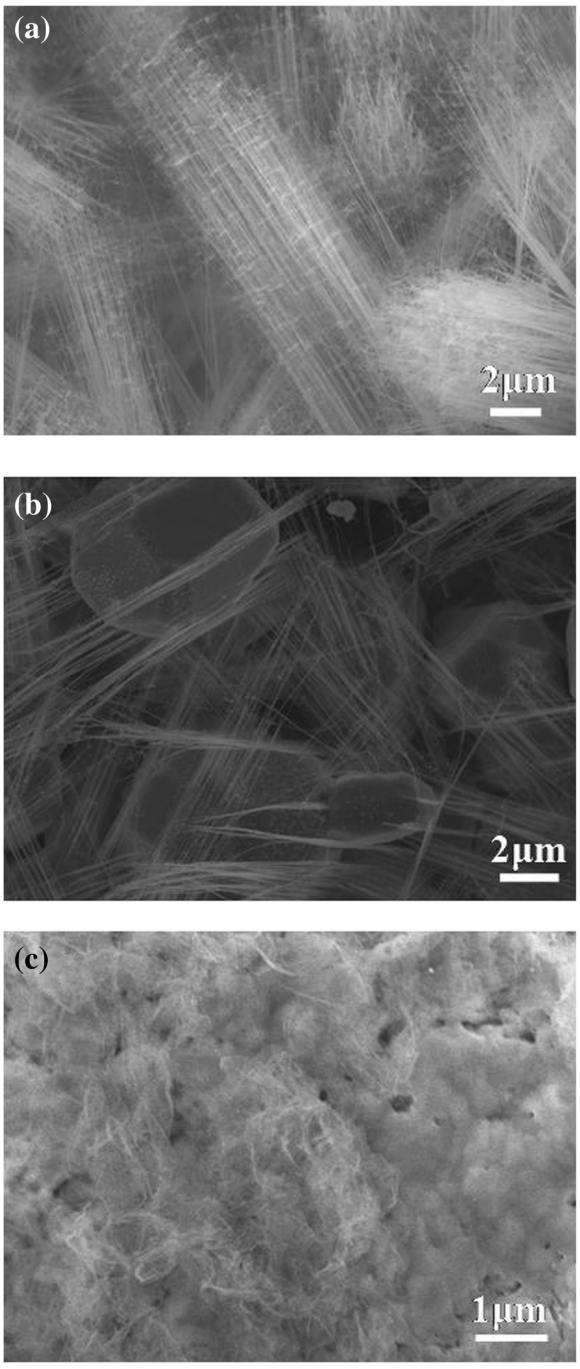

Figure 5 SEM images of $CrSi_2$ nanowires at different gas flow rates of (a) 60, (b) 120, and (c) 240 sccm, respectively.

[100] growth direction, and the interplanar spacing of plane (200) is 0.4571 nm.

The growth mechanism of the chromium silicide nanowires in this study is interesting. Figure 3 is the schematic illustration of the growth mechanism, showing the

proposed growth steps of the $CrSi_2$ nanowires. When the system was heated below 700°C, $CrCl_3 \cdot 6H_2O$ transformed to $CrCl_3$ and H_2O:

$$CrCl_3.6H_2O_{(g)} \rightarrow CrCl_{3(g)} + 6H_2O$$

The $CrCl_3$ gas molecules then agglomerated on the silicon substrate. As the system temperature reached the reaction temperature, 700°C, $CrCl_3$ gas reacted with the silicon substrate to form $CrSi_2$ nanoparticles and $SiCl_4$ based on step (1) of Figure 3:

$$4CrCl_{3(g)} + 11Si_{(s)} \rightarrow 4CrSi_{2(s)} + 3SiCl_{4(g)} \; T = 700°C$$

The $SiCl_4$ product then reacted with $CrCl_{3(g)}$ to form $CrSi_2$, following step (2) of Figure 3:

$$4SiCl_{4(g)} + 2CrCl_{3(g)} \rightarrow 2CrSi_{2(l)} + 11Cl_{2(g)} \; T = 700°C$$

Notably, the $CrSi_2$ nanowires precipitated from polygonal particles, and the growth direction seems consistent as shown in Figure 1b. The nanowires and polygonal particles may have the same stacking plane, (003), based on our TEM analysis, and nanowires grew from voids and defects on the surface of any polygonal particles with <001> growth direction, following step (3) of Figure 3 as shown in a SEM image of Additional file 1: Figure S1. We conducted experiments with the heating times of 1.5, 4, and 12 h at 700°C, obtaining the corresponding results shown in Figure 4a, b, c, respectively. We found nanowires and particles at 1.5 h, more nanowires growing from particles at 4 h, and dense nanowires appearing with buried particles at 12 h, respectively. With a longer duration, more nanowires can overcome the activation energy, successfully nucleate, and grow to be nanowires, contributing to $CrSi_2$ nanowires of a high density. According to the observations, we proposed that the mechanism of the nanowire growth is a self-catalytic process.

As the substrate temperature was at 750°C, $CrCl_3$ gas reacted with H_2 gas and the silicon substrate to form Cr_5Si_3 nanoparticles, HCl, and $SiCl_4$, following step (i) of Figure 3:

$$10CrCl_{3(g)} + 12Si_{(s)} + 3H_{2(g)} \rightarrow 2Cr_5Si_{3(s)} + 6SiCl_{4(g)} + 6HCl_{(g)} \; T = 750°C$$

The $SiCl_4$ also reacted with $CrCl_3$ to form $CrSi_2$, which is the reason why the XRD analysis shows both $CrSi_2$ and Cr_5Si_3 phases.

Also, we investigated the influence of the carrier gas flow rate when synthesizing chromium silicide nanowires. We conducted experiments at the gas flow rate of 60, 120, and 240 sccm at 700°C, obtaining the corresponding results shown in Figure 5a, b, c, respectively. It can be found that chromium disilicide nanowires appeared without particles at 60 sccm and with few particles at 120 sccm and that the morphology gradually transformed from nanowires to films at 240 sccm.

The CVD synthesis system can be divided into three sub-systems, which are momentum control system, mass transfer control system, and surface reaction control system. At a lower gas flow rate, mass transfer control system would be the main reaction mechanism, with which gas adsorption and desorption occurred on the Si wafer and fabrication of chromium silicide nanowires was preferred. On the other hand, at a higher gas flow rate, surface reaction control system would be the main reaction

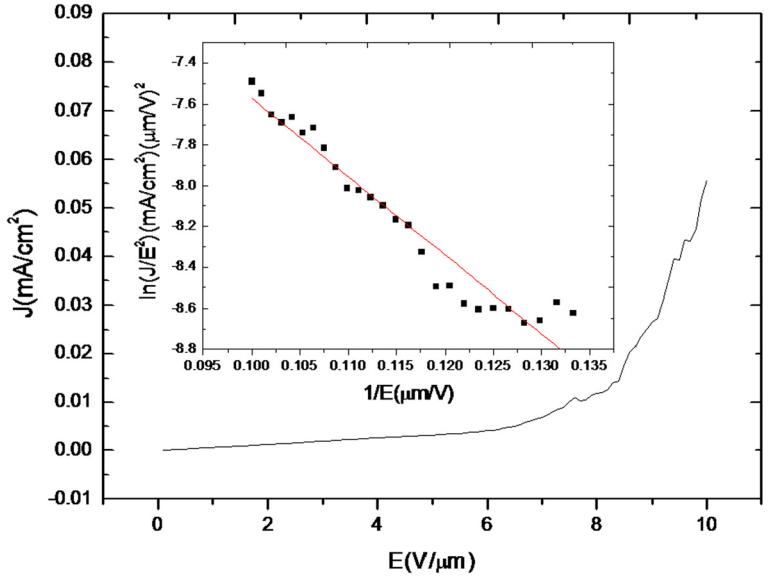

Figure 6 The field emission measurements of $CrSi_2$ NWs; the inset shows the corresponding $\ln(J/E^2)$-1/E plot.

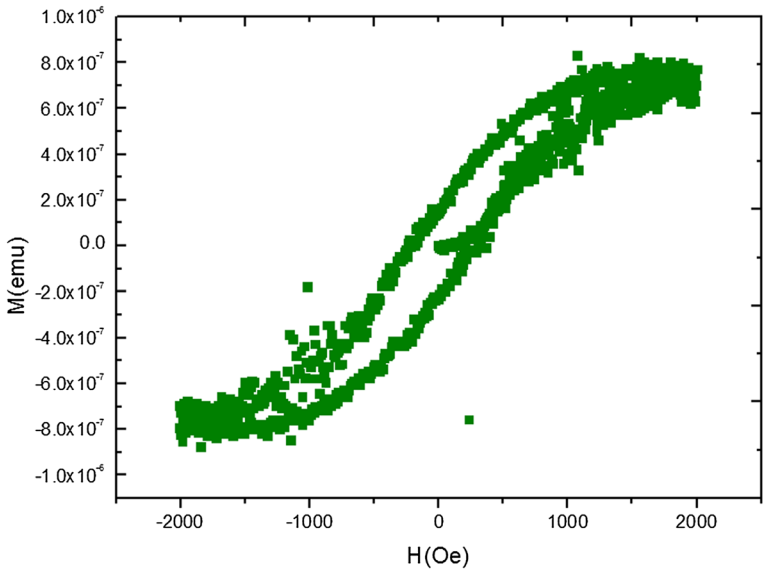

Figure 7 The magnetism measurements of $CrSi_2/SiO_x$ nanowires.

mechanism, with which $CrCl_3$ reacted on the Si wafer surface by chemical vapor deposition; thus, chromium silicide films appeared.

In addition to understanding the growth behaviors of the chromium silicide nanowires, we explored their physical properties. Figure 6 is the field emission measurements for $CrSi_2$ NWs, showing the plot of the current density (J) as a function of the applied field (E) with the inset of the $\ln(J/E^2)$-1/E plot. The sample was measured in a vacuum chamber pump to approximately 10^{-6} Torr. According to the Fowler-Nordheim (F-N) plot and the Fowler-Nordheim equation:

$$J = \left(A ß^2 E^2/\varphi\right) \exp\left(-B\varphi^{3/2}/ßE\right),$$

where J is the current density, E is the applied electric field, φ is the work function, and A, B are constants, respectively. We put +1,000 V on the sample with a 100-μm spacing between the anode and cathode, and we defined the turn-on field could obtain a current density of 10 μA/cm^2 and the turn-on field we measured for $CrSi_2$ nanowires was 7.5 V/μm. The field enhancement factor $ß$ has been calculated to be 1,366 from the slope of $\ln(J/E^2) = \ln(Aß^2/\varphi) - B\varphi^{3/2}/ßE$ (for $CrSi_2$, $\varphi = 3.9$ eV [19]), demonstrating that $CrSi_2$ NWs are promising emitters. The outstanding field emission properties of $CrSi_2$ NWs are attributed to their metallic property and special one-dimensional geometry with a high aspect ratio as compared with those of many other materials.

On magnetization analysis for chromium disilicide nanowires coated with a silicon oxide layer of a few nanometers in thickness, we prepared samples of 2.5 mm × 2.5 mm with the applied magnetic field of ±3,000 Oe perpendicular to the substrates. Notably, Figure 7 shows that the $CrSi_2/SiO_x$ nanowires grown here were found to be

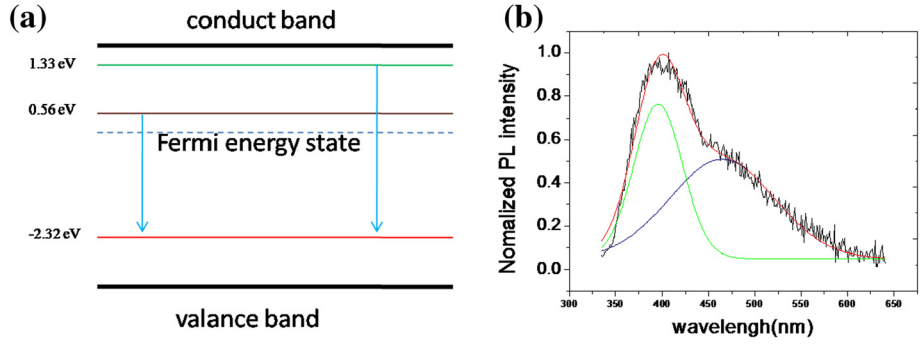

Figure 8 PL spectrum for the $CrSi_2$ nanowires. (a) Energy states of CrSi2 bulk. **(b)** Photoluminescence measurements of CrSi2 NWs with Gaussian fitting.

ferromagnetic with the saturation magnetization of 8×10^{-7} emu, M_R, remanence, of 2×10^{-7} emu, and H_C, coercive force, of about 179 Oe, respectively, which is different from the antimagnetic behavior in $CrSi_2$ and SiO_X. The ferromagnetic characteristic results from the bonding formation between the Si sp hybrid orbitals and the Cr 3d orbitals at the SiOx/$CrSi_2$ interface, where the oxygen atoms play an important role, bonding with silicon atoms and making chromium atoms with unpaired electrons, which contributes to ferromagnetism at nanoscale [25].

On photoluminescence analysis, Bhamu et al. studied the density of state (DOS) of $CrSi_2$ bulk, including 1.33 eV, 0.56 eV above Fermi state, and 2.23 eV under Fermi state [29]. Figure 8b shows our PL spectrum in the visible region for the $CrSi_2$ nanowires, where the wide peak was present (red line) and through Gaussian fitting; the other two peaks, 396 nm (green line) and 465 nm (blue line), were calculated. Theoretically, the electron-hole pair recombinations of 1.33 eV, 0.56 eV conduct state to −2.23 eV valance state were 348 and 430 nm for $CrSi_2$ bulk. In reality, the difference results from dimension, bulk, and nanowires; as the particle size reduces, wider bandgap light absorption band will move to shorter wavelengths, which is so-called blueshift [30]; however, there may be redshift as well; as the particle size decreases, the internal stress will increase, causing changes in the band structure [31] and the electron wave function overlap to increase the energy gap narrowing [32]; if the redshift factor is larger than the blueshift, then we will see redshift phenomenon, which is the case here.

Conclusions

In this study, using a CVD method, we have successfully synthesized chromium silicide nanowires of two phases with unique morphologies. Effects of some processing parameters, including the temperature, gas flow rate, and heating time, were investigated; for example, the growth of chromium disilicide nanowires were influenced by $CrSi_2$ vapor supersaturation, $CrSi_2$ vapor formation rate, and CVD control system. Also, the growth mechanism has been proposed. Field emission and photoluminescence measurements demonstrate that the $CrSi_2$ nanowires are potential field-emitting and photovoltaic materials with a low turn-on field. Additionally, the magnetic property measurements for the $CrSi_2/SiO_x$ nanowires, showing a ferromagnetic characteristic, demonstrate promising applications for magnetic storage and biological cell separation.

Additional file

Additional file 1: Figure S1. SEM image of $CrSi_2$ nanowires growing from voids and defects on the surface of silicide particles at 700°C.

Competing interests
The authors declare that they have no competing interests.

Authors' contributions
HFH and KCL conceived the study and designed the research. HFH conducted the experiments. HFH, PCT, and KCL wrote the manuscript. All authors read and approved the final manuscript.

Acknowledgements
KCL acknowledges the support from the National Science Council through grants 100-2628-E-006-025-MY2 and 102-2221-E-006-077-MY3.

Received: 10 December 2014 Accepted: 21 January 2015
Published online: 06 February 2015

References

1. Lu CM, Hsu HF, Lu KC. Growth of single-crystalline cobalt silicide nanowires and their field emission property. Nanoscale Res Lett. 2013;8:308.
2. Chiu WL, Chiu CH, Chen JY, Huang CW, Huang YT, Lu KC, et al. Single-crystalline δ-Ni2Si nanowires with excellent physical properties. Nanoscale Res Lett. 2013;8:290.
3. Lu KC, Wu WW, Ouyang H, Lin YC, Huang Y, Wang CW, et al. The influence of surface oxide on the growth of metal/semiconductor nanowires. Nano Lett. 2011;7:2753–8.
4. Wu WW, Lu KC, Chen KN, Yeh PH, Wang CE, Lin YC, et al. Controlled large strain of Ni silicide/Si/Ni silicide nanowire heterostructures and their electron transport properties. Appl Phys Lett. 2011;97:203110.
5. Wu WW, Lu KC, Wang CW, Hsieh HY, Chen SY, Chou YC, et al. Growth of multiple metal/semiconductor nanoheterostructures through point and line contact reactions. Nano Lett. 2010;10:3984–9.
6. Chou YC, Lu KC, Tu KN. Nucleation and growth of epitaxial silicide in silicon nanowires. Mat Sci Eng R. 2010;70:112–25.
7. Lu KC, Wu WW, Wu HW, Tanner CM, Chang JP, Chen LJ, et al. In situ control of atomic-scale Si layer with huge strain in the nanoheterostructure NiSi/Si/NiSi through point contact reaction. Nano Lett. 2007;8:2389–94.
8. Lu KC, Tu KN, Wu WW, Chen LJ, Yoo BY, Myung NV. Point contact reactions between Ni and Si nanowires and reactive epitaxial growth of axial nano-NiSi/Si. Appl Phys Lett. 2007;90:253111.
9. Liang YH, Yu SY, Hsin CL, Huang CW, Wu WW. Growth of single-crystalline cobalt silicide nanowires with excellent physical properties. J Appl Phys. 2011;110:074302.
10. Chen LJ. An integral part of microelectronics. JOM. 2005;57:24–30.
11. Derrien J, Chevrier J, Lethanh V, Mahan JE. Semiconducting silicide-silicon heterostructures: growth, properties and applications. Appl Surf Sci. 1992;382:56–8.
12. Ng WL, Lourenco MA, Gwilliam RM, Ledain S, Shao G, Homewood KP. An efficient room-temperature silicon-based light-emitting diode. Nature. 2001;410:192–4.
13. Leong D, Harry M, Reeson KJ, Homewood KP. A silicon/iron-disilicide light-emitting diode operating at a wavelength of 1.5 mum. Nature. 1997;387:686–8.
14. Bost MC, Mahan JE. An investigation of the optical constants and band gap of chromium disilicide. J Appl Phys. 1988;63:839–44.
15. Shinoda D, Asanabe S, Sasaki Y. Semiconducting properties of chromium disilicide. J Phys Soc Jpn. 1964;19:269–72.
16. Bellani V, Guizzetti G, Marabelli F, Piaggi A, Borghesi A, Nava F, et al. Theory and experiment on the optical properties of $CrSi_2$. Phys Rev B. 1992;46:9380–9.
17. Mattheiss LF. Electronic structure of $CrSi_2$ and related refractory disilicides. Phys Rev B. 1991;43:12549–55.
18. Anderson WA, Delahoy AE, Milano RA. 8 percent efficient layered Schottky-barrier solar cell. J Appl Phys. 1974;45:3913–5.
19. Bewlay BP, Lipsitt HA, Jackson MR, Chang KM. Processing microstructures and properties of Cr-Cr sub 3 Si, Nb-Nb sub 3 Si, and V-V sub 3 Si eutectics. Mater Manuf Processes. 1994;9:89–109.
20. Nishida I. The crystal growth and thermoelectric properties of chromium disilicide. J Mater Sci. 1972;7:1119–24.
21. Rowe DM. CRC handbook of thermoelectrics. Boca Raton, FL: CRC Press; 1995. p. 701.
22. Chung IJ, Hariz A. Surface application of metal silicides for improved electrical properties of field-emitter arrays. Smart Mater Struct. 1997;6:633–9.

23. Bonard JM, Salvetat JP, Stockli T, Forro L, Chatelain A. Field emission from carbon nanotubes: perspectives for applications and clues to the emission mechanism. Appl Phys A. 1999;69:245–54.
24. Minami T, Miyata T, Yamamoto T. Transparent conducting zinc-co-doped ITO films prepared by magnetron sputtering. Surf Coat Technol. 1998;108:583–7.
25. Hou TC, Han YH, Lo SC, Lee CT, Ouyang H, Chen LJ. Room-temperature ferromagnetism in $CrSi_2$(core)/SiO_2(shell) semiconducting nanocables. Appl Phys Lett. 2011;98:193104.
26. Zhang Y, Wu Q, Qian W, Liu N, Qin X, Yu L, et al. Morphology-controlled growth of chromium silicide nanostructures and their field emission properties. CrystEngComm. 2012;14:1659–64.
27. Seo K, Varadwaj KSK, Cha D, In J, Kim J, Park J, et al. Synthesis and electrical properties of single crystalline $CrSi_2$ nanowires. J Phys Chem C. 2007;111:9072–6.
28. Lee CT, Li TY, Chiou SH, Lo SC, Han YH, Ouyang H. First-principles analyses of unusual ferromagnetism observed in $CrSi_2$(core)/SiO_2(shell) nanocables. J Appl Phys. 2013;113:17E140.
29. Bhamu KC, Sahariya J, Ahuja BL. Electronic structure of ceramic CrSi2 and WSi2: Compton spectroscopy and ab-initio calculations. J Phys Chem Solids. 2013;74:765–71.
30. Wang Y, Herron N. Nanometer-sized semiconductor clusters: materials synthesis, quantum size effects, and photophysical properties. J Phys Chem. 1991;95:525–32.
31. Fu H, Zunger A. Electronic structure, surface effects, and the redshifted emission InP quantum dots. Phys Rev B. 1997;56:1496–508.
32. Smith CA, Lee HWH, Leppert VJ, Risbud SH. Ultraviolet-blue emission and electron-hole states in ZnSe quantum dots. Appl Phys Lett. 1999;75:1688–90.